THEORETICAL AND EXPERIMENTAL DETERMINATION OF EROSION RATE FOR SILVER CONTACTS UNDER 14 VDC

A. Lefort[(1)], M. Abbaoui[(1)], D. Sallais[(2)], N. Ben Jemaa[(3)], E. Carvou[(3)]

University Blaise Pascal, LAEPT Laboratory, 63177 Aubière, France[(1)] ,
Andre.Lefort@univ-bpclermont.fr[(1)], Mhammed.ABBAOUI@univ-bpclermont.fr[(1)]
Metalor Technologies (France) SAS, Contacts Division, BP 29, 28190 Courville-sur-Eure, France[(2)] ,
damien.sallais@univ-rennes1.fr[(2)]
University of Rennes 1, PALMS Laboratory, 35042 Rennes, France[(3)] ,
noureddine.ben-jemaa@univ-rennes1.fr[(3)] , erwann.carvou@univ-rennes1.fr[(3)]

Abstract : **Erosion rate of electrical contacts is a fundamental parameter to understand and evaluate the performances of contact materials and their breaking devices such as the life time. In this study, we have focused our interest on the erosion in automobile applications under the 14 VDC power network.**

The experimental apparatus, adapted to perform contact breaking in similar conditions to the automotive relays, ensures arc duration control by artificial quenching, with a constant arc current close to 40 A. Erosion rates of the electrodes were determined by weighing before and after 5000 breaking operations..

In parallel, theoretical study based on a finite element calculation is conducted. A three-dimension simulation gives erosion volumes and liquid volume evolution versus time.

To improve erosion resistance and avoid welding of the silver contacts at make, composites with additives, a one-dimension simulation was made to calculate erosion rate of such contact materials, except for $AgSnO_2$.

Keywords: **silver contacts, erosion, contact material phase changes, silver metal-oxide alloys.**

1. Introduction

Anode and cathode erosion rates in switches and relays are fundamental parameters to improve breaking device life time. The most common measurement of erosion is the mass change of the contacts, determined by weighing of the electrodes, before and after electrical tests. In this work, we attempt to determine erosion rate under 14 VDC, 40 A, by finite element simulation and by taking into account mass transfer between the anode and the cathode.

A time dependant anode thermal flux combined with a variable cathode spot repartition were considered to evaluate the mass exchanges between electrodes and liquid and vapor volumes evolution versus time, and were compared to experimental results.

These calculations were led, first with a 3D axisymetric geometry for Ag contacts, and then extended to metal oxides ZnO and CdO with a 1D model.

2. Experimental results

2.1. Test equipment and procedures

The experimental apparatus is a fully automated device which has been widely described in previous paper [1,2]. It is adapted to perform contact breaking in similar conditions to the industrial switches and relays. It is mainly composed of an electrical module (power supply, variable resistance and inductance) and of a mechanical part (stepping motor) which insures the separation between the moving contact (cathode) and the fixed contact (anode) with a controlled constant speed v in the range 1-50 cm/s. The main measuring instrument is a digital scope which samples and stores arc voltage V_a and arc current I_a during the break.

In addition, a parallel thyristor has been used to ensure arc duration control by artificial arc quenching. This latter component is gated at a given time T_d after arc ignition (figure 1) and stopped the arc discharge.

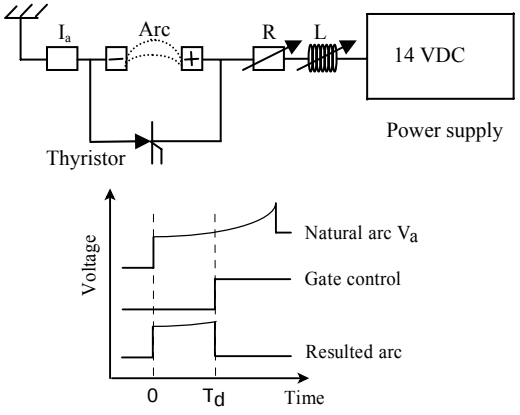

Fig. 1: Synoptic of the apparatus.

978-2-84516-363-8/07/$25.00 © 2007
Blaise Pascal Academic Press

An high inductive load of 50 mH (time constant L/R = 140 ms >> T_d) keeps constant arc current close to 40 A, as it is shown in figure 2. This allows us to consider the field of bilateral erosion (bilateral losses of the anode and the cathode).

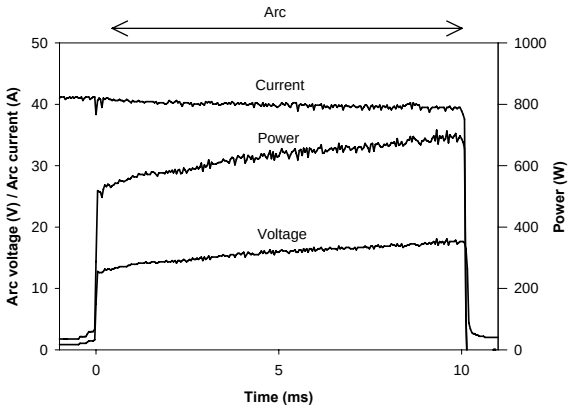

Fig. 2: Voltage, current and power characteristics of an arc adjusted to T_d=10 ms, 14 VDC, 40 A, 20cm/s.

Contact materials used for this study are pure silver rivets (figure 3). The anode is flat while the cathode is bombed (10 mm radius).

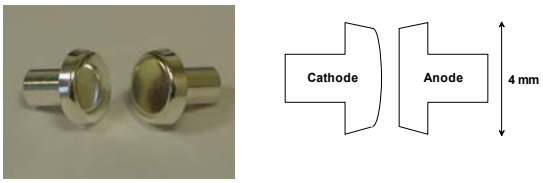

Fig. 3 : Silver rivets.

2.2. Silver erosion.

Experiments were performed for a wide arc length range (from 1 µm to 2000 µm). This allows us to consider the different fields of material transfer [3]: anodic (from the anode to the cathode), then in the reverse direction with a cathodic mass transfer (from the cathode to the anode), and at last the bilateral erosion for high arc lengths (bilateral losses of the both electrodes).

For each arc duration T_d , the same contacts pair performs 5000 operations under arc on break and null current on make in the following conditions: 14 VDC, 40A, opening speed of 20cm/s. Anodic and cathodic mass variations are determined by micro-weighing and averaged over three tests. Figure 4 shows the mass variations of anode and cathode versus arc length for pure silver.

3. Theoretical analysis and simulations

In this part, authors have focused their interest on the thermal flux received by the electrode surface at the junction with the electrical arc. For the anode, energy is mainly transmitted by electrons, while for the cathode, metallic ions resulting for metallic vapour ionization , transfer energy to the electrode surface.

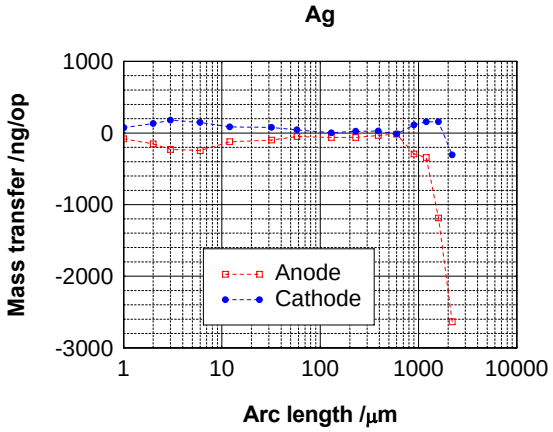

Fig. 4 : Mass transfer evolution versus arc length for pure silver contacts, 14 VDC, 40 A, 20cm/s.

3.1. Theoretical analysis

3.1.1. Anode energy flux

In the electric arc the anode spot collects the column electrons, JD Cobine and EE Burger [4] give an energy flux equation on the anode electrode surface:

$$P_{anode} = J_a \times (V_a + \varphi + V_T) + P_n + P_r \qquad (1)$$

where J_a is the anode current density, V_a the anode voltage drop, φ the material work function, P_n the result of the energy of neutral atoms and P_r the radiant energy from the column. Usually the two last parts of equation 1 are negligible in comparison with the first part, V_T results of electron column flux. The incoming flux P_{anode} is transmitted to the anode surface, the part $P_{thermal}$ is transmitted to the electrode material, the part P_{es} is used to the emission of secondary electrons, and P_{rs} correspond to the photon emission so:

$$P_{anode} = P_{thermal} + P_{es} + P_{rs} \qquad (2)$$

It is commonly admitted that the parts of the power used by the secondary electron emission, and by the material radiation are negligible comparatively to the power transmitted to the electrode. Approximations give:

$$P_{thermal} = J_a \times (V_a + \varphi + V_T) \qquad (3)$$

3.1.2. Cathode energy flux

At the cathode, the energy flux balance [5] gives:

$$P_{cathode} = P_{ion} = P_{thermal} + P_{ec} + P_{rs} \qquad (4)$$

where P_{ion} is the energy flux delivered to the cathode surface by the ions coming from the plasma

978-2-84516-363-8/07/$25.00 © 2007
Blaise Pascal Academic Press

sheath. The energy flux P_{ec} is the result of the electron emission, but is negligible in comparison with $P_{thermal}$ [6] . Conclusions are similar for P_{rs}. The flux P_{ion} is given by [5]:

$$P_{ion} = (1-s)\times(V_c + V_i - \varphi)\times J_c \qquad (5)$$

V_c represents the cathode voltage fall, V_i the ionisation potential, J_c the total cathode current density and s represents the part of current resulting from the electron flux. With the approximations made above, the thermal power flux density $P_{thermal}$ directed on the cathode material surface is equal to the power flux P_{ion} given by the equation 5.

3.1.3. Conduction of heat in contacts

The electrode surface receives at the junction with the electric arc the thermal flux $P_{thermal}$ Energy is transmitted to the electrode material and dissipated by thermal conduction, by melting and vaporisation. To obtain the material solid-liquid-vapour and temperature evolution in each point , we solve, the enthalpy form heat equation contact, versus time t:

$$\frac{\partial H}{\partial t} = div(k\vec{\nabla}T) + Source \qquad (6)$$

H, k and T represent respectively material enthalpy, thermal conductivity and temperature.
The figure 5 precises the geometry used: the electrode is a Oz – axis cylinder; at time $t = 0$, the thermal flux is applied on a circular surface whose centre is located at $z = 0$ with a radius equal to r_a.

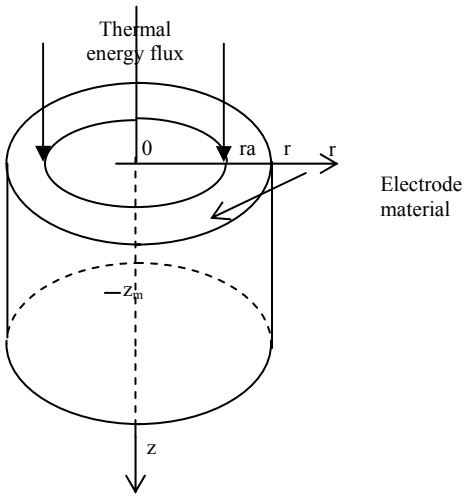

Fig. 5: The thermal energy flux is applied to the cylindrical electrode.

The numerical method is described in the paper of Rossignol [7] about 1D simulation. In 3D axisymetric simulation, energy is transmitted in the Oz and Or directions instead of only in Oz direction. At $t = 0$, each point is at room temperature with a specific enthalpy equal to H_0. Then with the transmission of the energy by conduction starting from the surface circle, H involves to reach successively the specific liquefaction enthalpy and the specific vaporisation enthalpy liquid and vapour volumes appear. It gives versus time the liquid and the vapour volume evolution, erosion is defined by the vapour volume amount. Nevertheless this definition needs to be discussed in the comparison with experimental results. The studied domain is limited by the coordinate $z = z_m$ and $r = r_m$, the surfaces defined by these coordinates obey to the condition $H = H_0$.

3.2. Experimental results – Discussion

First, figure 4 shows that erosion and material transfer already occurs at the beginning of the contacts separation (for a few micrometers).

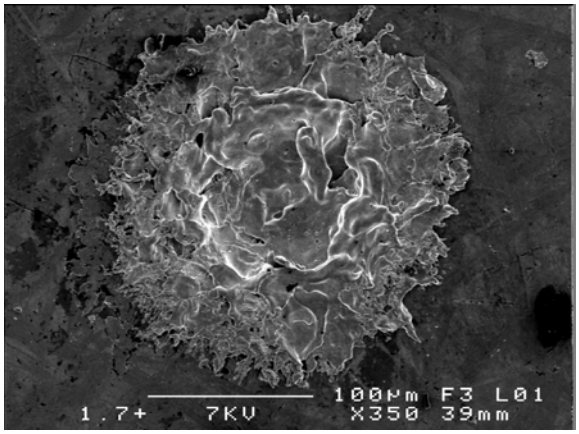

Anode

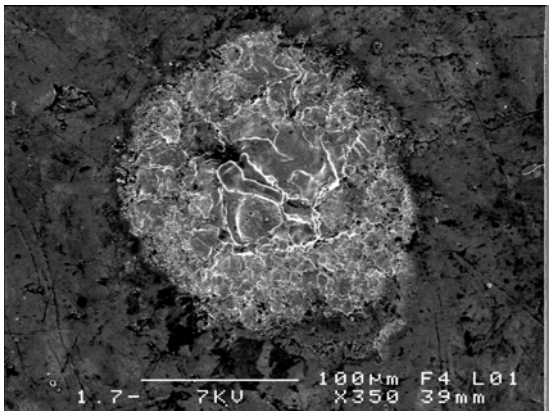

Cathode

Fig. 6: Anode and cathode spot surface for an arc length of 1.7 µm. Eroded areas exhibits a medium diameter of 109 µm for the anode and 91 µm for the cathode.

978-2-84516-363-8/07/$25.00 © 2007
Blaise Pascal Academic Press

Microscopic observations, presented in figure 6, confirm this result. For such contacts separation values, we can't consider a single cathode spot, but a multispots distribution. The difference of surface area between the both eroded areas provides the influence radius of one cathode spot. With such a geometric analysis, we find 40 emission spots of 1 A each one. For the higher contacts separation distances, theoretical calculations are led with only one emission spot of 40 A.

To calculate the parameters defined in the paragraph 3.1, we consider, according experimental results shown in figure 4, that the anode erosion flux is equal to the cathode erosion flux. As the anode spot surface area does not evolve during the contacts separation, parameters for the anode are deduced from this assumption. Calculation gives then the erosion flux values. However, this method does not permit to determine the erosion rate presented in figure 9 for low time values (below $3.8\times10^{-4}\,s$). New cathode spot characteristics have also to be developed.

3.3. Parameters used for simulation

3.3.1. Anode parameters

With a defined anode surface area, a defined arc current value, and with Te the medium temperature of electrons moving from the arc column towards the anode surface, the anode power flux is given by :

$$P_{thermal} = 1.07\times10^{9}\times(V_a + 2kT_e + 4.63)$$

4.63 V corresponds to the extraction work of electrons for silver. To satisfy the conditions defined in the paragraph 3.2, it is necessary to impose : $V_a + 2kT_e = 2V$. In this case, the energy flux received by the anode spot is equal to $7.107\times10^{9}\,Wm^{-2}$. However, this calculated energy flux value, uniform in time and space, leads to a vapor emission (responsible from material transfer) from the anode to the cathode starting from a time of $20\times10^{-6}\,s$. This result is not in good agreement with the experimental value (figure 4). Vaporization occurs earlier, so at the beginning of contacts separation, during the $40\times10^{-6}\,s$, the power density should be higher, time dependant and r-coordinates dependant, i.e. :

$t \le 3\mu s$

$$P_{thermal} = 4.4216\times10^{10}\times(1-\frac{r^2}{1.881\times10^{-8}})$$

$3\mu s \le t \le 4\mu s$

$$P_{thermal} = (1.34234\times10^{11} - 3.0006\times10^{16}\times t)\times(1-\frac{r^2}{1.881\times10^{-8}})$$

$4\mu s \le t \le 40\mu s$

$$P_{thermal} = 1.421\times10^{10}\times(1-\frac{r^2}{1.881\times10^{-8}})$$

$t \ge 40\mu s$

$$P_{thermal} = 7.107\times10^{9}\,Wm^{-2}$$

With such parameters, we consider that there is only a very few number of cathode spots (or no cathode spots) during the first microseconds (corresponding to an electrodes separation of about 1 µm). The main part of the dissipated power is received by the anode surface. After $40\mu s$, the gap between the contacts, equal to $8\mu m$, allows the development of cathode spots.

3.3.2. Cathode parameters

According to the equation 5 (paragraph 3.1.2) and to the following parameters for silver: electronic fraction (s=0.8), cathode fall ($V_c = 12.3V$), ionization potential ($V_i = 7.56V$), and electrons extraction work ($V_s = 4.63V$), the power flux transmitted to the cathode is only depending from current density J_c : $P_{ions} = 3.05\times J_c$.

Erosion values defined in the paragraph 3.3.1 and results presented figure 4 lead to two kinds of cathode spots, allowing each one a current intensity of 1 A:

- in the contacts gap range : [0 µm (contacts closed) – 76 µm] :

$J_c = 5\times10^{11}\,Am^{-2}$; $r_c = 0.7979\mu m$;

$P_{ions} = 1.5246\times10^{12}\,Wm^{-2}$

- in the contacts gap range : [76 µm – 240 µm] :

$J_c = 1.3\times10^{12}\,Am^{-2}$; $r_c = 0.4948\mu m$;

$P_{ions} = 3.9640\times10^{12}\,Wm^{-2}$.

Calculations were not made for contacts gaps higher than 240 µm. In this case, the cathode spots number deacreases up to one cathode spot, which insures the passage of a current of 40 A.

3.4 Simulation results

Figure 7 shows the solid-liquid and liquid-vapor transformed volumes versus arc duration, for a cathode spot with a current density equal to $J_c = 1.3\times10^{12}\,Am^{-2}$.

We can note on this figure, that anode and cathode exhibit similar behaviors: as the electrodes surfaces receive a thermal flux, first a liquid phase appears before vaporization. For short gaps, the emitted vapor is recovered by the opposite electrode. By using, for

978-2-84516-363-8/07/$25.00 © 2007
Blaise Pascal Academic Press

exchanged flux, the results obtained with conditions described in paragraphs 3.3.1 and 3.3.2, we deduce the cathode mass profit. Theoretical and experimental results are presented figure 8. They are in good agreement.

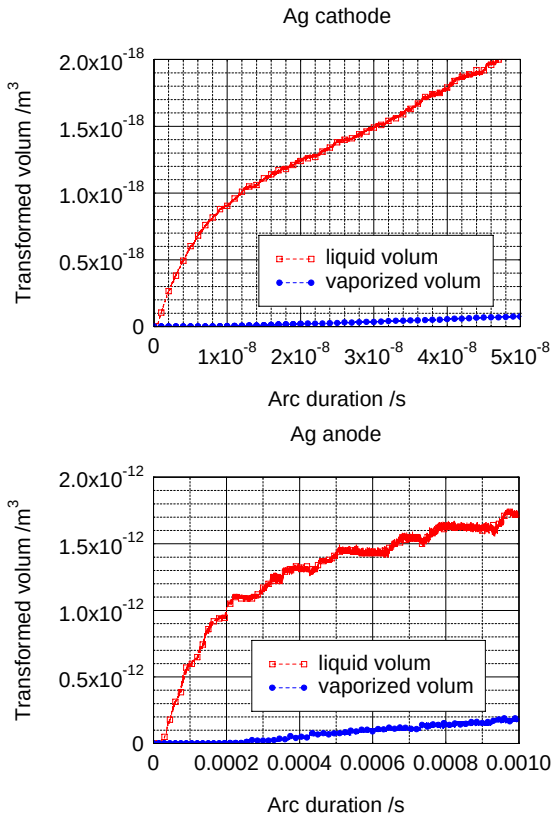

Fig. 7: Cathode and anode vaporized and liquefied volume evolution.

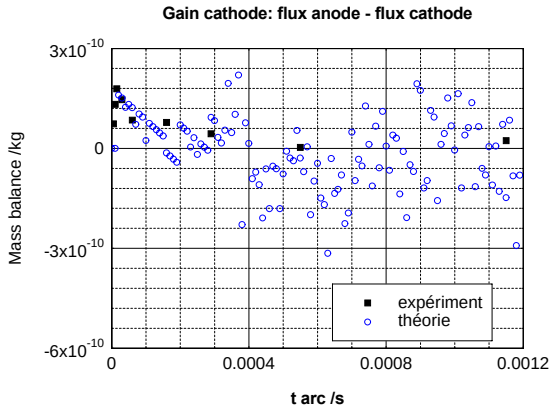

Fig.8: Comparison between theoretical and experimental results for the cathode.

4. Case of AgMeO

4.1 Simulation

Oxides grains disseminated in the Ag-matrix, exhibits an undefined form of a few micrometers, whatever the elaboration process. In spite of their low electrical conductivity, they receive ions or electrons from the thermal flux transmitted to the electrodes, because of their small dimensions, either about arc root surface size for the cathode, or very lower than the anode spot area. By taking into account this assumption, a 3D-simulation of heating and phase changes for oxide grains is not necessary. In this work, a 1D-simulation was also realized to compare the both oxide ZnO and CdO with silver. Theoretical results are presented figure 9, for a thermal flux density in the range [1.10^{11} W m^{-2} - 5.10^{12} W m^{-2}] for the cathode, and in the range [5.10^{8} W m^{-2} - 1.10^{10} W m^{-2}] for the anode.

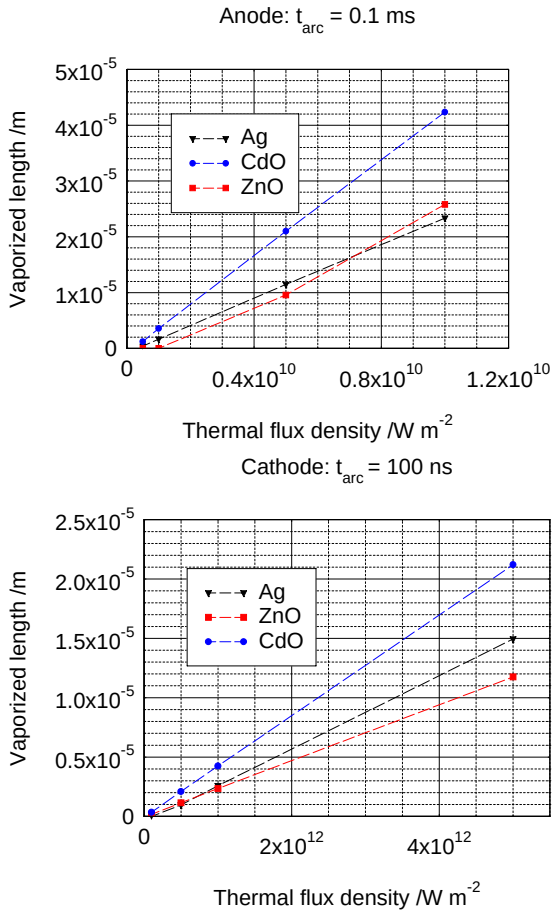

Fig. 9: Thickness of silver films and oxides films vaporized under arcing at the anode and the cathode.

First, we can note similar evolutions for oxides and silver. And the same behaviour is observed on the figure 10, which presents the vaporization speed versus thermal flux density, when only the vaporization is taken into account.

Simulation shows clearly, that the values obtained for silver are framed by those of both oxides. In addition, CdO exhibits a lower resistance against thermal flux in comparison with Ag and ZnO.

978-2-84516-363-8/07/$25.00 © 2007
Blaise Pascal Academic Press

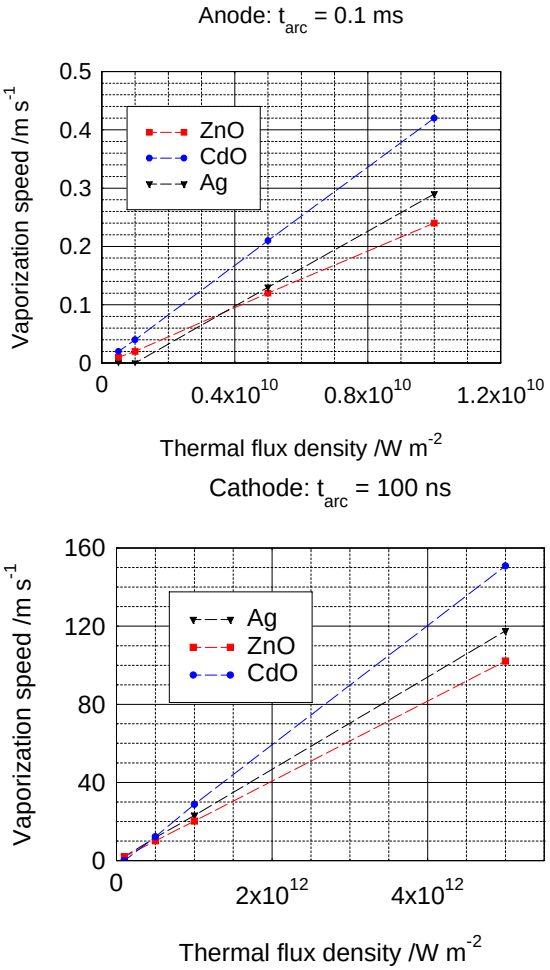

Fig. 10: Anode and cathode vaporization speed for Ag, CdO and ZnO.

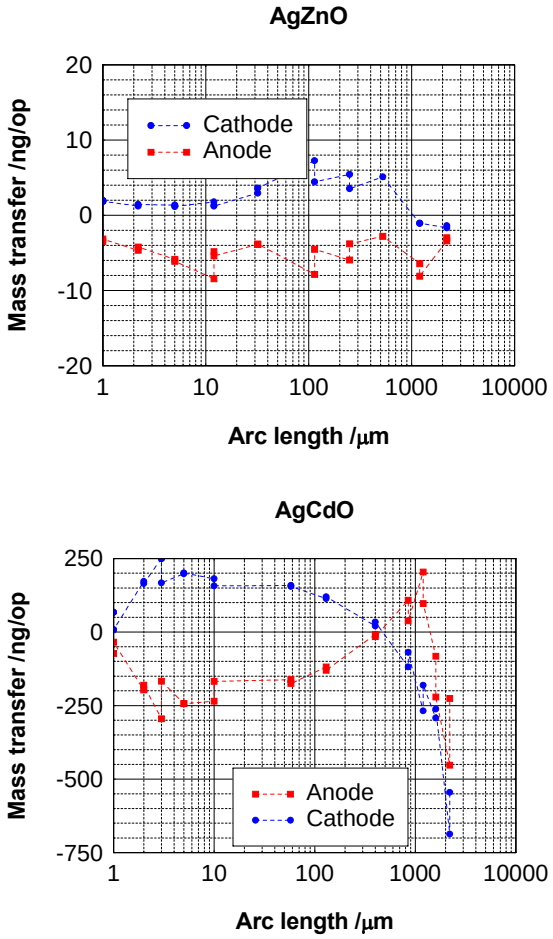

Fig. 11: Material transfer evolution versus arc length, for contacts in AgZnO and AgCdO.

4.2. Comparison with experimental results

Experimental results for pure silver and composites AgCdO and AgZnO are shown figures 9 and 10.

Experimental and theoretical results from figures 9, 10 and 11 show, that AgZnO exhibits the lowest transfer rates in comparison with Ag and AgCdO which transfers the largest amount of material.

5. Conclusion

The 3D finite element simulation for Ag contacts under 14 VDC and 40 A, leads to material transfer and erosion rates in good agreement with experimental results. To improve anti-welding properties, metal oxides, such as SnO_2, ZnO, and CdO (nowadays forbidden for environmental requirements) are usually added to Ag-matrix in electrical contacts. Simulation for SnO_2 could not be carried out, because of the lack of physical constants for this oxide. However, a 1D calculation provide in this paper vaporization speed of ZnO and CdO, which bring response elements in the understanding of the behaviour of the composites AgMeO.

References

[1] N. Ben Jemaa, L. Nedelec, S. Benhenda, "Break arc duration and contact erosion in automotive application", IEEE Trans. CPMT, vol.19, no.1, March 1996, pp.82-86.

[2] N. Ben Jemaa, L. Doublet, L. Morin, D. Jeannot, "Break arc study for the new electrical level of 42 V in automotive applications", Proc. 47th IEEE Holm Conf. On EC, Montreal, Sept. 2001, pp.50-55.

[3] N. Ben Jemaa, L. Morin, S. Benhenda, L. Nedelec, "Anodic to cathodic arc transition according to break arc lengthening", IEEE Trans. CPMT, vol.21, no.4, December 1998, pp.599-603.

[4] Cobine J.D. and Burger E.E. "Analysis of Electrode Phenomena in the High-Current Arc", J. Appl. Phys., Vol 26 , 1955, pp.895-8.

[5] Lee T.H. and Greenwood A. "Theory of the Cathode Mechanism in Metal Vapour Arc", J. Appl. Phys. Vol 33, 1961, pp.916-23.

[6] Lee T.H. "Energy Distribution and Cooling Effect of Electrons Emitted from an Arc Cathode", J. Appl. Phys., Vol. 31, 1960, pp. 924-7.

[7] Rossignol J., Abbaoui M. and Clain S. "Numerical modelling of thermal ablation phenomena due to a cathodic spot", J. Phys. D : Appl. Phys. Vol. 33, 2000, pp. 2079-86.

978-2-84516-363-8/07/$25.00 © 2007
Blaise Pascal Academic Press